Australian Journal of Earth Sciences (2000) **47**, 1053–1064

Petrological, geochemical and geochronological evidence for a Neoproterozoic ocean basin recorded in the Marlborough terrane of the northern New England Fold Belt*

M. C. BRUCE, Y. NIU, T. A. HARBORT AND R. J. HOLCOMBE

Department of Earth Sciences, University of Queensland, Qld 4072, Australia.

Petrological, geochemical and radiogenic isotopic data on ophiolitic-type rocks from the Marlborough terrane, the largest (~700 km^2) ultramafic–mafic rock association in eastern Australia, argue strongly for a sea-floor spreading centre origin. Chromium spinel from partially serpentinised mantle harzburgite record average Cr/(Cr + Al) = 0.4 with associated mafic rocks displaying depleted MORB-like trace-element characteristics. A Sm/Nd isochron defined by whole-rock mafic samples yields a crystallisation age of 562 ± 22 Ma (2σ). These rocks are thus amongst the oldest rocks so far identified in the New England Fold Belt and suggest the presence of a late Neoproterozoic ocean basin to the east of the Tasman Line. The next oldest ultramafic rock association dated from the New England Fold Belt is *ca* 530 Ma and is interpreted as backarc in origin. These data suggest that the New England Fold Belt may have developed on oceanic crust, following an oceanward migration of the subduction zone at *ca* 540 Ma as recorded by deformation and metamorphism in the Anakie Inlier. Fragments of late Neoproterozoic oceanic lithosphere were accreted during progressive cratonisation of the east Australian margin.

KEY WORDS: Marlborough terrane, Neoproterozoic, New England Fold Belt, ocean basin.

INTRODUCTION

The Marlborough terrane, or Marlborough Block of Holcombe *et al.* (1997a,b), of the northern New England Fold Belt contains a large (~700 km^2) ultramafic–mafic complex, the largest rock association of its kind in eastern Australia. In his regional surveys, Murray (1969, 1974) pointed out that this complex may be of ophiolitic origin, but very little was known about its petrology and geochemistry, let alone the timing and tectonic environment in which this complex may have developed.

In this paper, we present petrological, geochemical and isotopic data on the complex and show that it represents fragments of oceanic lithosphere formed at a sea-floor spreading centre. This new finding is a departure from the typical arc-related ophiolitic-type rocks from other parts of the fold belt (Aitchison *et al.* 1994). Furthermore, a mafic whole-rock Sm/Nd isochron age of 562 ± 22 Ma (2σ) points to the presence of a late Neoproterozoic ocean basin.

REGIONAL GEOLOGICAL FRAMEWORK

The New England Fold Belt of eastern Australia is a ~2000 km-long tectonic collage composed largely of Palaeozoic subduction/accretion elements and Late Palaeozoic extensional basins overprinted by contractional elements of the Permo-Triassic Hunter–Bowen Orogeny (Leitch 1974). Early plate-tectonic models postulated a long-lived Andean-type margin that involved the migration of an arc front with the present margin always in a forearc position (Leitch 1975; Day *et al.* 1978; Cawood & Leitch 1985). More recent studies and new observations have suggested that the present margin was located in both the forearc and backarc/foreland positions at different intervals (Aitchison *et al.* 1992; Aitchison & Ireland 1995; Holcombe *et al.* 1997a,b; Allen *et al.* 1998; this study). The New England Fold Belt developed on or against elements of the Tasman Orogenic Zone that cratonised earlier in Cambrian and Ordovician times. The New England Fold Belt itself underwent a major fold-thrust orogenic event at the end of the Permian (Hunter–Bowen Orogen: Leitch 1974).

The Marlborough terrane is located in the northern New England Fold Belt (Figure 1) within a marked oroclinal flexure in the Permo-Triassic fold-thrust belt. The terrane (Figure 2) is a fault-bounded, near-horizontal, out-of-sequence thin-skinned nappe sheet (Holcombe *et al.* 1997a; Korsch *et al.* 1997). Thrust-imbricated slices consist of an ultramafic–mafic complex, upper and lower greenschist facies metasedimentary units (quartz–feldspar–mica schist, banded quartzite), and lower amphibolite facies S-type metagranite and metabasite. Permo-Triassic I-type granites intrude these units (Figure 2). The metasedimentary units comprise rocks that are similar to the Devonian–Carboniferous accretionary coastal terrane units (Holcombe *et al.* 1997a). A strong foliation in the S-type metagranites is attributed to deformation associated with intercalation of these rocks with the ultramafic–mafic complex, an event that occurred prior to final emplacement of the terrane during the Hunter–Bowen Orogeny.

The ultramafic–mafic complex consists of four serpentinite thrust sheets that are dominated by serpentinised

*Fuller versions of Tables 1 and 2 are Supplementary Papers lodged with the National Library of Australia (Manuscript Section); copies may be obtained from the Business Manager, Geological Society of Australia.

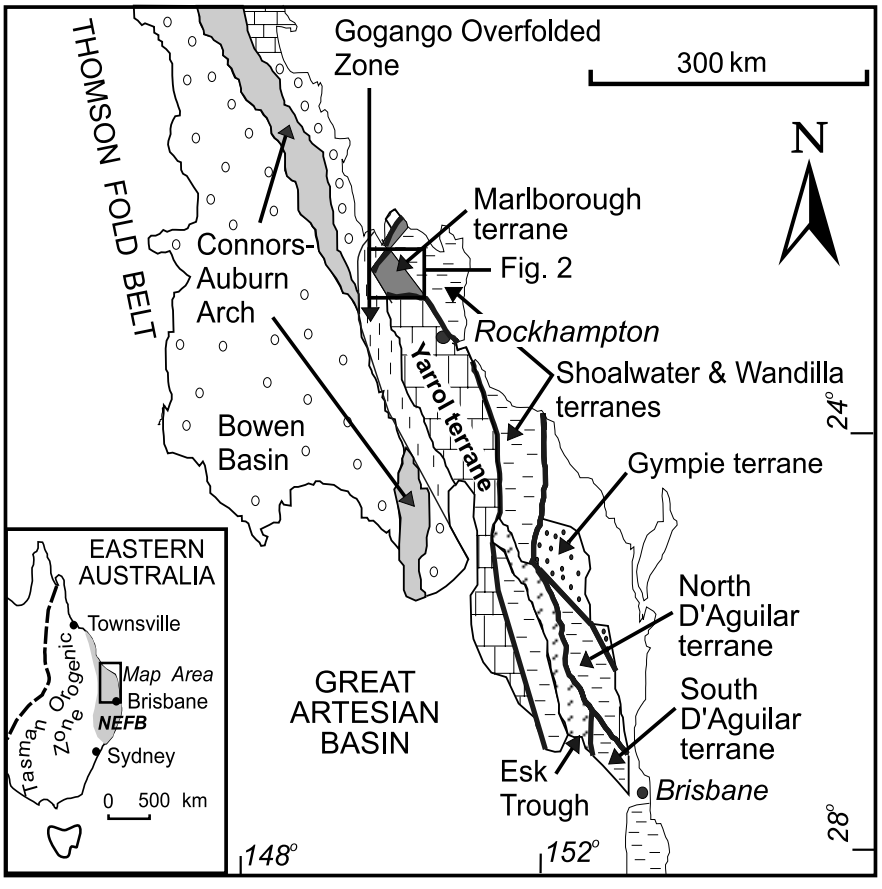

Figure 1 Simplified tectonic map of the northern New England Fold Belt (NEFB) showing the location of the Marlborough terrane (Figure 2). Inset indicates the location of map area within the NEFB, which is the easternmost tectonic unit of the Tasman Orogenic Zone of eastern Australia.

mantle harzburgite with minor dunite and pyroxenite. The serpentinite is largely massive with localised cleaved zones, mainly in regions disrupted by late (Cretaceous and Tertiary) normal faulting, and strongly schistose zones near the contacts with surrounding units. The bases of the serpentinite sheets are metamorphosed from upper greenschist to amphibolite facies and generally display high angle, ductile thrusting with east-over-west shear sense indicators. Incorporated in the serpentinite thrust sheets are numerous chromitite pods, metagabbros and associated basaltic enclaves, dykes, and other mafic and minor felsic intrusions.

PETROLOGY OF ULTRAMAFIC–MAFIC ROCKS

The Marlborough ultramafic–mafic complex is composed of rocks that represent the products of four tectonomagmatic events. The oldest event comprises elements of an ophiolite. These elements include serpentinised harzburgite, podiform chromitite, isotropic gabbro and various basaltic intrusions. The rocks associated with the 'younger' events are discussed in Bruce and Niu (2000).

Representative analyses of minerals (olivine, orthopyroxene, clinopyroxene and chromium spinel) in the major lithologies are presented in Table 1 (the locations of all samples mentioned in the tables are given in Appendix 1). Minerals were analysed for major elements including Ni and Cr using a JEOL Superprobe JXA-8800L at the University of Queensland. Analytical conditions were optimised for standard silicates including Ni and Cr at 15 kV accelerating voltage with a 20 nA focused electron beam for all the elements with the exception of Na and K for which a broader beam (10 μm) was used. Routine analyses were obtained by counting 30 s at peak and 5 s on background. Repeated analysis of natural and synthetic mineral standards yielded precisions better than 1% for all the major oxides analysed (SiO_2, TiO_2, Al_2O_3, FeO, MnO, MgO, CaO, Na_2O, K_2O, Cr_2O_3 and NiO). Instrumental drift was corrected for by repeatedly analysing standards as unknowns during the run. FeO/Fe_2O_3 ratios were calculated for spinel assuming perfect stoichiometry and end-member proportions.

Serpentinised harzburgite

Serpentinised mantle peridotite comprises about 95% of the ophiolitic body. A dominant tectonite harzburgite protolith is apparent from partially serpentinised peridotite (Denton 1994; this study) with features characteristic of alpine-type peridotite (Thayer 1967). However, for the most part, primary mineralogy has been entirely replaced or pseudomorphed by serpentine with only scattered relicts remaining. Estimated primary modal abundances for the harzburgite are ~75% olivine, ~20% enstatite, ~4% diopside and ~1% spinel. Minor pyroxenite cumulate and dunite (Murray 1969) also exist in the harzburgite.

The Marlborough serpentinites can be divided into three classes on the basis of microscopic texture: pseudomorphic, transitional, and non-pseudomorphic (O'Hanley 1995).

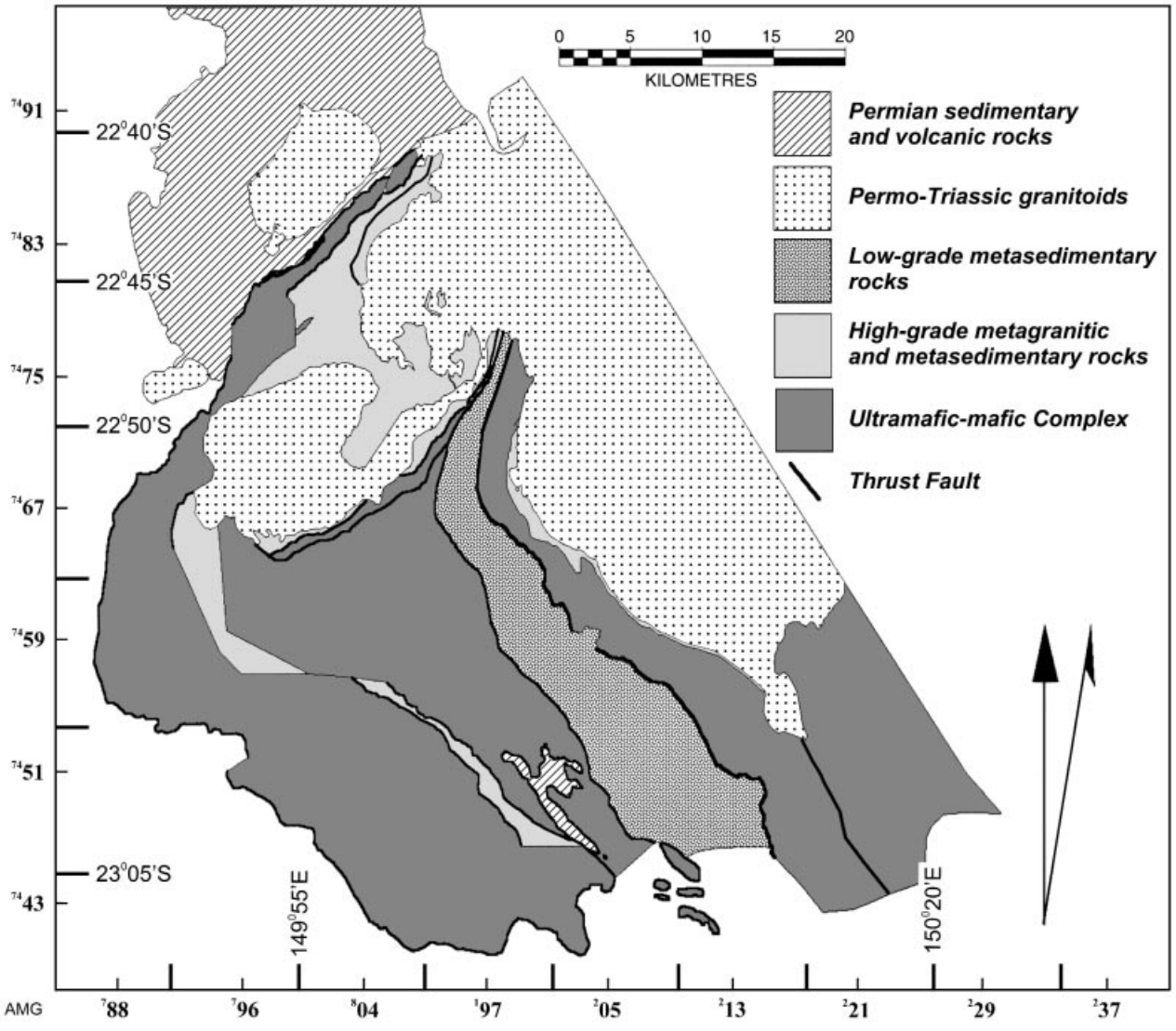

Figure 2 Simplified geological map of the Marlborough terrane. Grid is from Marlborough, Rookwood (AMG Zone 55) and Princhester (AMG Zone 56) 1:100 000 topographic maps. See Figure 1 for location.

PSEUDOMORPHIC SERPENTINITES

A proportion of the unstructured, coherent serpentinite has survived a regional metamorphic overprint and retains the original (sea floor) serpentine mineralogy. Mesh cells and ribbons of lizardite dominate the texture of these rocks. Mesh cells usually consist of low birefringent serpentine with relicts of igneous olivine ($Fo_{90.5–91.5}$) present in some samples. Elongated laths of lizardite/chrysotile define the cell rims. Networks of magnetite grains around former olivine boundaries (Murray 1969) locally preserve the original granular texture. Enstatite bastites are typically 1–3 mm in size and usually retain their pyroxene cleavages. Relics of clinopyroxene are also present in some samples. In most instances they appear to have survived serpentinisation, but are heavily altered to talc and often display magnetite lamellae parallel to the original c-axis cleavage planes. Chrome spinel is present and commonly consists of unaltered cores surrounded by 'ferro' chrome rims. Cr# [Cr/(Cr + Al)] in the unaltered cores ranges from 0.32 to 0.47, well within the array defined by modern abyssal peridotites (Dick & Bullen 1984) (Figure 3). Partially serpentinised samples contain igneous olivine (av. $Fo_{91.1}$), enstatite crystals ($En_{87–91}$), interstitial diopside ($Wo_{44–49}$) and chromium spinel (av. Cr# = 0.38). The Al_2O_3% content in the pyroxenes overlaps the field defined by modern harzburgites from the major oceanic basins (Hébert *et al.* 1989) (Figure 4).

TRANSITIONAL SERPENTINITES

The remainder of the unstructured, coherent serpentinites have experienced prograde metamorphism. These serpentinites have textures transitional between pseudomorphic and non-pseudomorphic textures (Wicks & O'Hanley 1988; O'Hanley 1995). They include type-2 (O'Hanley 1995) hourglass textures composed predominantly of lizardite and chrysotile and interlocking textures of chrysotile and antigorite. Enstatite bastites are commonly pseudomorphed by plastically deformed ribbons of lizardite. Clinopyroxene crystals are altered to talc and usually enclose small magnetite grains in a poikiolitic texture.

Table 1 Representative microprobe analyses of olivine, orthopyroxene, clinopyroxene and chromium spinel from the Marlborough harzburgites, chromitites and gabbros.

	Olivine	Orthopyroxene	Clinopyroxene		Chromium Spinel	
	MB94	MB88	MB94	MB100	MB18	MB108
	Harzburgite	Harzburgite	Harzburgite	Gabbro	Harzburgite	Chromitite
SiO_2	40.97	55.41	52.72	52.68	0.00	0.00
TiO_2	0.00	0.03	0.11	0.42	0.03	0.13
Al_2O_3	0.00	3.50	4.39	2.12	32.78	36.44
Cr_2O_3	0.02	1.03	1.33	0.14	36.07	32.68
Fe_2O_3	–	–	–	–	1.85[a]	3.27[a]
FeO^T	8.92	5.74	2.27	5.79	14.20[a]	9.27[a]
MnO	0.10	0.17	0.11	0.19	0.22	0.18
MgO	50.03	33.26	17.12	16.94	14.62	18.73
CaO	0.01	1.09	21.64	21.45	–	–
Na_2O	0.00	0.00	0.49	0.30	–	–
K_2O	0.00	0.00	0.01	0.01	–	–
NiO	0.34	0.06	0.06	0.04	0.12	0.18
Total	100.39	100.31	100.24	100.08	99.90	100.88
Si	0.9970	1.9104	1.9036	1.925	–	–
Ti	0.0000	0.0007	0.0029	0.012	0.0007	0.0028
Al	0.0000	0.1423	0.1870	0.091	1.1336	1.2040
Cr	0.0003	0.0282	0.0381	0.004	0.8369	0.7242
Fe^{2+}	0.1815	0.1555[b]	0.0685[b]	0.124[b]	0.3486[a]	0.2173[a]
Fe^{3+}	0.0000	0.0100[b]	0.0000[b]	0.053[b]	0.0408[a]	0.0689[a]
Mn	0.0020	0.0049	0.0032	0.006	–	–
Mg	1.8151	1.7094	0.9216	0.923	0.6395	0.7827
Ca	0.0001	0.0403	0.8370	0.840	–	–
Na	0.0000	0.0000	0.0341	0.021	–	–
K	0.0000	0.0000	0.0006	0.000	–	–
Ni	0.0067	0.0018	0.0017	0.001	–	–
Total	3.0028	4.0036	3.9983	4.000	3.0000	3.0000
Cr#	–	–	–	–	0.42	0.38
Mg#	0.91	0.92	0.93	0.88	0.65	0.78

Olivine and spinal ions on the basis of 4 oxygen, pyroxene ions on the basis of 6 oxygens.
FeO^T = total iron.
[a]Calculated from stoichiometry.
[b]Calculated by charge balance following International Mineralogical Association guidelines (Gomez Cebria 1990).
Mg# = Mg/(Mg + Fe^{2+}).
Cr# = Cr/(Cr + Al).

Locally, networks of magnetite grains are found to rim former olivine crystals. Prismatic to acicular crystals of tremolite up to 2 mm long (usually < 0.5 mm) are also present in some samples. Chrome spinel is variably altered to 'ferro' chrome compositions.

NON-PSEUDOMORPHIC SERPENTINITES

Locally, schistose serpentinites display non-pseudomorphic textures with well-orientated blades of interpenetrating and/or interlocking antigorite crystals. Variable amounts of prograde mosaic, subrounded and elongated metamorphic olivine (Fo_{95}) and talc partially pseudomorph antigorite. Pyroxene bastites have frequently lost their original texture with triangular antigorite blades replacing lizardite, although in a few samples ribbon serpentine survived. Clinopyroxene crystals have been altered to talc and usually display magnetite veining oriented along former c-axis cleavage planes. Needles of tremolite/anthophyllite are also common in these rocks. Relict chrome spinel is ubiquitous in these rocks, but it is entirely altered to 'ferro' chrome compositions.

Podiform chromitite

Small chromite bodies occur scattered throughout the serpentinite units. Chromitites are generally massive and podiform in texture with chromite grains interspersed with gangue material.

In thin-section, chromite is reddish-brown and highly fractured with opaque chromite defining the fracture zones. Chromium spinel is homogeneous and unaltered with high Mg# (av. 0.76). The TiO_2 content in the chromium spinel ranges from 0.13% to 0.30%, which is well within the range for oceanic gabbros, and significantly higher than in residual harzburgites (< 0.09%) as expected. Cr# ranges from 0.37 to 0.44.

The gangue material consists of serpentine ± talc ± tremolite occurring in stretching veinlets and interstitial patches between chromite grains and makes up between < 10% and 60% of the samples. Serpentine is usually antigorite replacing lizardite after olivine, suggesting a chromite–olivine cumulate origin. Locally, the gangue mineral is lizardite pseudomorphing pyroxene.

Isotropic gabbro

Metamorphosed isotropic (non-layered) gabbro occurs as fault-bounded blocks within the serpentinite. The primary igneous mineralogy is apparent on outcrops and in hand specimens characterised by interlocking crystals of clinopyroxene and plagioclase in approximate ratio of 2:1. Grainsize varies from 1 to 20 mm with an average of 4–5 mm. Clinopyroxene retains partial to complete primary igneous textures, is diopsidic in composition (Table 1) and is similar in TiO_2 content (av. 0.40%) to clinopyroxene in gabbros from other ophiolites such as Yakuno and Canyon Mountain (Ishiwatari 1985). The general increase in clinopyroxene Ti content with decreasing Mg# is consistent with varying degrees of fractional crystallisation. Clinopyroxene compositions lie in the field of oceanic gabbros on a Ti *vs* Cr diagram (Hébert *et al.* 1989) (Figure 5). Plagioclase is commonly altered to albite, but where primary it is labradorite in composition ($An_{54–57}$). The gabbros are overprinted by a metamorphic assemblage of hornblende + actinolite + partially saussuritised albite ± prehnite–pumpellyite ± chlorite ± carbonate ± quartz ± epidote ± sphene. Locally, anorthite veins crosscut the metagabbros, which grade into Ca-metasomatised rodingites with anorthite partially saussuritised and pseudomorphed by hydrogrossular.

Basaltic pockets interpreted to represent trapped melt occur in the metagabbros. These enclaves are fine grained, volumetrically insignificant (< 0.5 m in diameter) and largely composed of metamorphic hornblende and plagioclase. Minor amounts of secondary actinolite, quartz, chlorite and sphene are present.

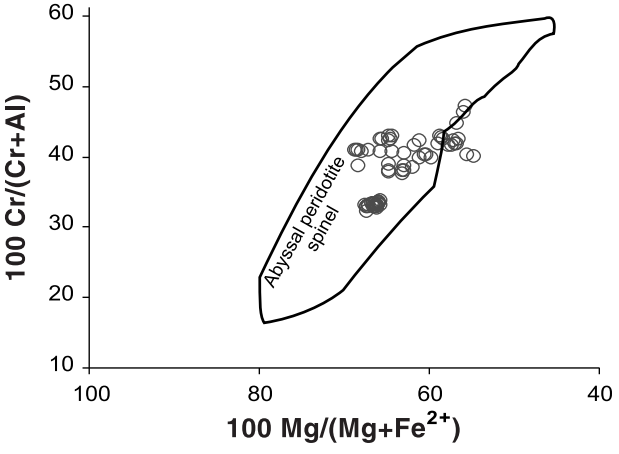

Figure 3 Cr/(Cr + Al) *vs* Mg/(Mg + Fe^{2+}) diagram for chromium spinels of the Marlborough harzburgites. Field of abyssal peridotite spinel after Dick and Bullen (1984).

Basaltic intrusions

Fine- to medium-grained mafic dykes metamorphosed to amphibolite facies locally intrude the serpentinite. Metamorphism to amphibolite facies was probably caused by nearby granitoid stock intrusion. The amphibolites display total recrystallisation from original basaltic mineralogy to homogeneous subrounded grains of hornblende/tremolite alternating with layers of rounded quartz, calcite, plagioclase and minor amphibole defining a gneissosity that is evident under the microscope, but not always obvious in hand specimens.

Some fine-grained doleritic dykes also intrude isotropic gabbros. These dykes are also metamorphosed, and have a greenschist facies assemblage (hornblende + actinolite + albite + chlorite ± quartz ± carbonate ± sphene), with chromium spinel (Cr# = 0.37) being the only relict igneous mineral.

GEOCHEMISTRY

Analytical techniques

MAJOR ELEMENTS

Analyses of representative samples are presented in Table 2. Samples were crushed in a TEMA tungsten-carbide mill. Major elements (SiO_2, TiO_2, Al_2O_3, Fe_2O_3T, MnO, MgO, CaO, Na_2O, K_2O and P_2O_5) for ultramafic rocks were determined using glass fusion discs by X-ray

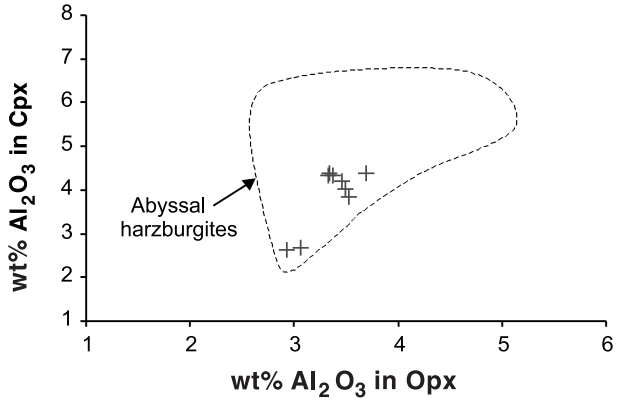

Figure 4 Al_2O_3 partitioning between clinopyroxene (Cpx) and orthopyroxene (Opx) in harzburgites of the Marlborough ophiolite. Dashed line indicates field of abyssal harzburgites after Hébert *et al.* (1989).

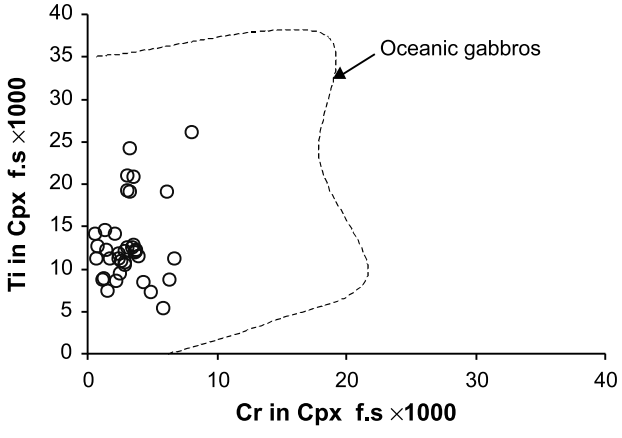

Figure 5 Ti *vs* Cr diagram for clinopyroxenes (Cpx) of the Marlborough gabbros. Dashed line indicates field of oceanic gabbros (Hébert *et al.* 1989). f.s, number of cations in structural formula.

fluorescence (XRF) on a Phillips PW1400 at the University of Queensland. Ni and Cr were analysed using pressed-powder pellets and mass absorption corrections were applied (Norrish & Chappell 1977). Loss on ignition (LOI) was determined by placing 1 g of sample in a furnace at 1000°C for several hours, cooling in a desiccator, and reweighing. Analytical errors for major element oxides are < 0.5% for oxides with > 10 wt%, and 1–3% for oxides < 10 wt% based on repeated analyses on USGS reference standard PCC-1 and DTS-1 and for Ni and Cr ≤ 1–2% for elements ≥ 100 ppm and ~5% for elements < 100 ppm. Major elements of non-ultramafic rocks were determined using Inductively Coupled Plasma-Atomic Emission Spectroscopy (ICP-AES) at Queensland University of

Table 2 Major and trace-element analyses of harzburgites and mafic rocks from the Marlborough ophiolite.

	MB21 Harzburgite	MB88 Harzburgite	MB94 Harzburgite	MB3 Dolerite	MB8 Basalt	MB9 Gabbro	MB114 Gabbro	MB116a Dolerite
SiO_2	43.16	40.82	40.78	46.37	49.29	50.24	46.92	44.79
Al_2O_3	0.84	0.89	0.88	0.29	0.82	0.44	0.27	0.88
TiO_2	0.02	0.01	0.02	17.82	15.34	14.61	15.66	15.06
$Fe_2O_3^T$	8.11	8.27	7.67	6.44	9.01	5.97	5.63	9.68
MnO	0.12	0.12	0.13	0.14	0.14	0.10	0.14	0.17
MgO	33.67	41.16	42.04	12.09	9.68	10.59	9.48	12.86
CaO	0.08	1.64	0.99	15.26	12.51	13.46	21.39	14.60
Na_2O	0.00	0.30	0.35	1.68	2.23	2.79	0.49	1.52
K_2O	0.00	0.00	0.01	0.09	0.10	0.06	0.08	0.14
P_2O_5	0.00	0.00	0.00	0.05	0.10	0.11	0.06	0.10
NiO	0.36	0.43	0.35	–	–	–	–	–
Cr_2O_3	0.31	0.28	0.29	–	–	–	–	–
LOI	13.27	6.77	7.77	1.03	1.79	1.79	0.90	1.34
Total	99.97	100.69	101.28	101.26	101.01	100.16	101.03	101.14
Li	5.17	1.86	0.90	8.13	15.1	15.13	6.06	4.03
Be	0.004	0.008	0.021	0.17	0.14	0.33	0.05	0.21
Sc	8.98	12.13	9.41	36.33	33.43	38.54	30.91	32.87
V	29	39.71	27.89	143.7	198	112.7	123.3	167
Cr	–	–	–	499	326	611	480	809
Co	113.4	108.5	110	37.09	42.97	36.8	32.03	63.53
Ni	–	–	–	167	100.3	161	127.4	400
Cu	2.14	7.97	9.53	13.13	40.36	35.91	30.81	13.45
Zn	44.72	38.68	31.52	31.89	34.27	27.96	25.83	51.91
Ga	0.78	0.75	1.05	12.2	12.85	10.01	10.15	11.01
Rb	0.205	0.064	0.159	1.3	0.8	0.99	1.36	0.23
Sr	2.08	5.26	7.69	108.7	54.46	172	36.38	36.21
Y	0.69	0.15	0.27	8	18.27	28.95	6.45	17.94
Zr	0.01	0.02	0.04	8.43	43.45	61.54	6.73	45.60
Nb	38.01	30.9	47.9	0.15	1.09	2.13	0.1	0.31
Cs	71.49	11.1	11.9	0.05	0.19	0.13	0.13	0.01
Ba	51298	394	2069	18.35	7.21	9.32	5.13	6.46
La	352	0.6	16.9	0.39	1.16	2.63	0.24	0.99
Ce	35.75	0.4	23.2	1.29	4.17	8.98	0.84	4.04
Pr	108.8	1	3.3	0.26	0.82	1.61	0.17	0.82
Nd	508	2	8.8	1.58	4.74	8.56	1.06	4.73
Sm	119.1	5.4	9.5	0.67	1.82	3.01	0.48	1.81
Eu	34.8	1.5	2.5	0.47	0.73	0.7	0.32	0.68
Gd	167.2	3.9	14.9	1.14	2.68	0.8	0.17	2.54
Tb	16.36	1.6	4.1	0.2	0.49	4.23	0.84	0.47
Dy	100.4	16.9	37	1.43	3.38	5.52	1.23	3.27
Ho	25.28	5.9	11.9	0.3	0.74	1.2	0.28	0.72
Er	79.12	25.2	40.6	0.91	2.12	3.46	0.79	2.13
Tm	11.34	6	7.9	0.13	0.31	0.52	0.13	0.32
Yb	82.24	45.5	54.2	0.82	1.98	3.20	0.79	2.08
Lu	15.76	8.3	10.9	0.12	0.3	0.48	0.12	0.32
Hf	***	2.2	3.6	0.29	1.3	2	0.24	1.29
Ta	22.86	9.1	9.1	0.03	0.07	0.15	0.01	0.03
Pb	44.67	38.4	83.5	1.2	0.16	0.43	5.18	1.43
Th	2.13	0.6	38.8	0.01	0.07	0.28	0.01	0.02
U	58.67	0.1	0.9	0.003	0.02	0.04	0.00	0.008

$Fe_2O_3^T$ = total iron; major elements analysed by X-ray fluorescence (XRF) and Inductively Coupled Plasma-Atomic Emission Spectrometry (ICP-AES), trace elements analysed by Inductively Coupled Plasma-Mass Spectrometry (ICP-MS); ***, concentration in blank was larger than in sample; concentration of trace elements in ppm, except for Li to Zr in the three harzburgite samples, which are in ppb.

Technology. Analyses were performed on a Varian Liberty 200 spectrometer, following the procedure of Kwiecien (1990). Accuracy (1σ) for most elements based on USGS standards (BCR-1, BIR-1, AGV-1 and G2) is < 1% with the exception of TiO_2 (1.3%) and P_2O_5 (2.0%).

TRACE ELEMENTS

Analyses of representative samples are presented in Table 2. Fine-grained samples were crushed in a soft-steel percussion mill and sieved down to a size of 500 μm to minimise trace contamination from the TEMA mill associated with powders. The coarser plutonic samples were powdered in a TEMA chromium-steel mill to enable a representative portion of the rock to be analysed. Trace elements were analysed on a Fisons VG PlasmaQuad 2 Inductively-coupled Mass Spectrometer at the University of Queensland. All waters used were Milli-Q® and all acids were double-distilled. A HF–HCl–HNO_3 mixture was added to 50–100 mg of sample in a Savillex® Teflon® beaker, capped and left overnight on a hotplate at 150°C. The dissolved sample was evaporated to incipient dryness and a HNO_3–HCl mixture was added, followed by evaporation at 150°C. This process was repeated a further three times using only concentrated HNO_3. A HNO_3–H_2O mixture was then added and left capped overnight on a hotplate at 100°C. Internal standards (In, Re, Tl) were added and the final solution diluted to a total dissolved solid of 0.1%. A blank and at least two of the USGS reference rock standards (BIR-1, AGV-1, PCC-1 and W-2) were prepared in the same way and analysed concurrently with the samples. In addition to the internal standards, one sample was repeatedly analysed to monitor instrumental drift and appropriate corrections were made. All samples were analysed at least three times.

Alteration

Most studies into the mobility of elements during alteration and metamorphism of volcanic rocks have concluded that the major elements, with the exception of TiO_2, are suspect in terms of their primary chemical characteristics (Cann 1969; Pearce 1976). Likewise, the large-ion lithophile elements (LILE: such as K, Rb, Cs, Sr, Ba, Pb and U) are also mobile. In general, the high-field strength elements (HFSE: such as Ti, Nb, Ta, Zr and Hf) and the rare-earth elements (REE: La, Ce, Pr, Nd, Sm, Eu, Gd, Tb, Dy, Ho, Er, Tm, Yb, Lu plus Y) are immobile in aqueous fluids (Campbell *et al.* 1984; Lesher *et al.* 1986), except for a few light REE (LREE) in certain circumstances such as high water/rock ratios and carbonate alteration (Humphris 1984).

The rocks of the Marlborough ultramafic–mafic complex have been variably serpentinised and metamorphosed to greenschist facies with variable carbonate alteration. However, primary igneous signatures are relatively well-preserved for most HFSE and REE. In some rocks, metamorphic sphene is present, probably due to the breakdown of rutile and ilmenite during an influx of carbonate-rich fluid. However, this reaction is simply a Ti redistribution, and does not introduce gain or loss of this element in the whole-rock system (Niu & Lesher 1991).

RESULTS

Variation in extent of melting or modal mineralogy should result in correlated variations between major elements in residual harzburgite (Niu 1997; Niu *et al.* 1997). Such covariations, however, are absent in the Marlborough harzburgites on plots such as MgO *vs* SiO_2 or MgO *vs* Ni, suggesting that serpentinisation and subsequent metamorphism and alteration did affect these elements. For example, a reasonable approximation of MgO loss can be seen in a MgO/SiO_2 *vs* Al_2O_3/SiO_2 plot (Figure 6), assuming that Al_2O_3 and SiO_2 were immobile or less mobile. The loss in MgO is a function of the vertical displacement from the terrestrial array (Snow & Dick 1995).

Chondrite-normalised REE distributions for representative samples of the Marlborough mantle harzburgites are shown in Figure 7. Based on REE patterns, the harzburgites can be divided into three distinct groups: Group 1, LREE-depleted (Figure 7a); Group 2, LREE-enriched with U-shaped patterns (Figure 7b); and Group 3, LREE-enriched with elevated middle-REE (MREE) abundances (Figure 7c). Mantle peridotites have long been considered to be dominantly LREE depleted (Haskin *et al.* 1966) and this is the case with the Group 1 Marlborough harzburgites. However, many REE patterns from mantle harzburgite from ophiolite complexes display LREE enrichments or U-shaped chondrite-normalised distributions (Frey 1984) similar to those of the Group 2 Marlborough harzburgites. These U-shaped REE patterns appear to be restricted to harzburgites and lherzolites that give the most refractory bulk chemistry ($Al/Si < 0.05$) and the most refractory diopside compositions ($TiO_2 < 0.25$: Gruau *et al.* 1998). The Marlborough harzburgites are sufficiently depleted ($Al/Si < 0.02$ and TiO_2 content in diopside < 0.12) and thus their LREE-enriched distributions are typical of these types of rocks. Group 3 Marlborough harzburgites are not only enriched in LREE, but also in MREE abundances. Frey

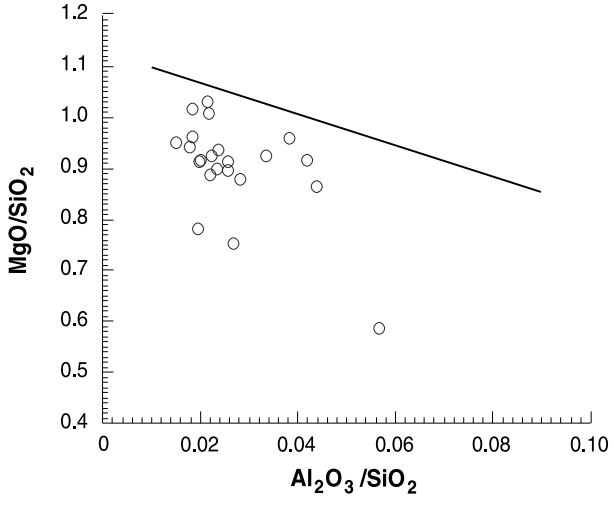

Figure 6 MgO/SiO_2 *vs* Al_2O_3/SiO_2 for Marlborough harzburgites. Line shows the location of the 'terrestrial array' (Jagoutz *et al.* 1979). Note that samples plot below the terrestrial array, indicating loss of MgO, assuming that nothing else (particularly Al_2O_3 and SiO_2) is removed from or added to the rock during weathering (Snow & Dick 1995).

(1984) suggested that the MREE enrichments could be due to the crystallisation of accessory amphibole, which is observed in petrographic thin-sections of these particular samples. However, residual harzburgites contain such a small amount of MREE that the presence of minor amphibole would not satisfactorily explain the observed enrichments.

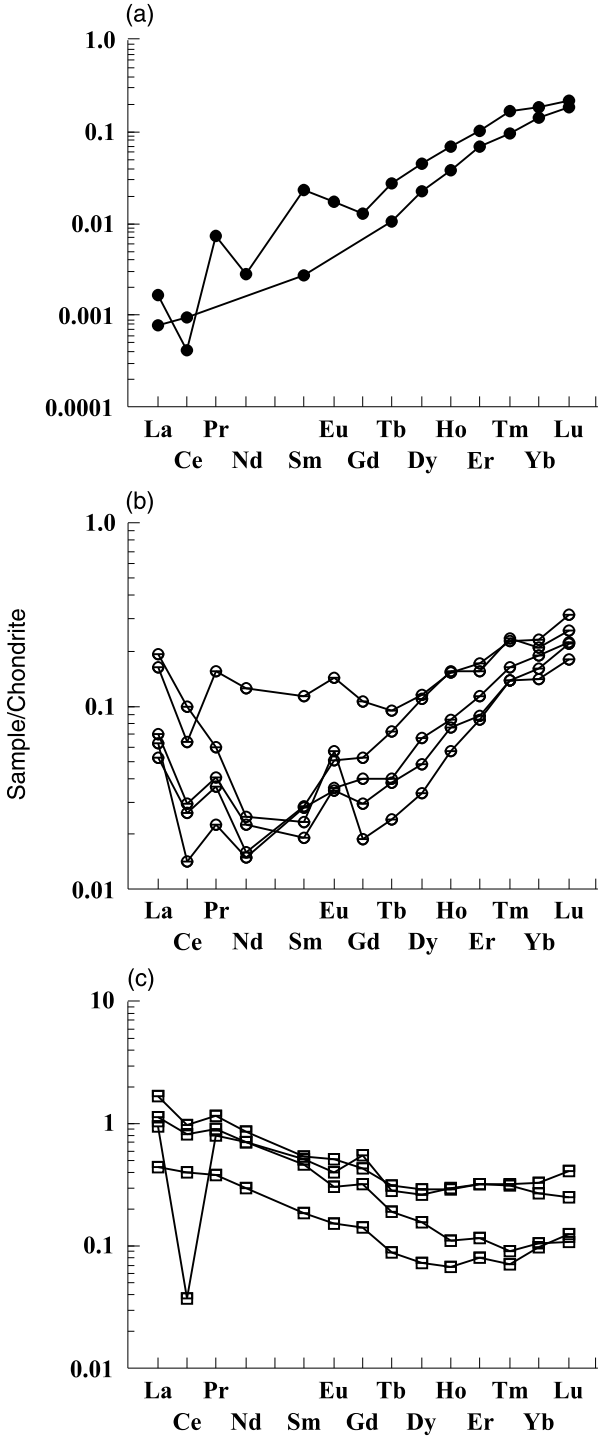

Figure 7 Chondrite-normalised rare-earth element (REE) patterns for the Marlborough harzburgites. Note that there are three distinct groupings based on light REE enrichment/depletion: (a) Group 1; (b) Group 2; (c) Group 3. The negative Ce anomalies are due to weathering.

There are three possible explanations for enrichment in LREE in mantle peridotites: (i) refertilisation of depleted harzburgites by melt interaction (Niu & Hékinian 1997); (ii) mantle metasomatism (Frey 1984; Bodinier 1990); or (iii) contamination from crustal-derived fluids (Gruau *et al.* 1998). A detailed examination of these three explanations is outside the scope of this paper, however, the processes that readily account for the REE distributions in the Marlborough harzburgites are: (i) simple melting residues for the Group 1 harzburgites; (ii) modification of the Group 2 harzburgites by a depleted melt of hydrothermal fluids; and (iii) refertilisation of the Group 3 harzburgites by a LREE-enriched melt.

The isotropic gabbros have an average $Mg/(Mg + Fe^{2+})$ ratio of 0.75. This value is unlikely to reflect primary ratios, as Mg enrichment has accompanied the secondary formation of metamorphic minerals (e.g. hornblende and actinolite). CaO/Al_2O_3 is variable, ranging from 0.7 to 1.4, with the higher values (i.e. > 1) correlating with the petrographic observation of calcium metasomatism. Calcium mobility is indicated by the occurrence of rodingites and anorthite veins partially pseudomorphed by hydrogrossular observed in some samples. The amphibolite facies mafic dykes have a high $Mg/(Mg + Fe^{2+})$ ratio of 0.8, consistent with Mg enrichment, and a CaO/Al_2O_3 ratio of 1:1, consistent with the petrographic observation of carbonate formation.

Plots of incompatible trace elements in the mafic rocks normalised to N-MORB are shown in Figure 8. Despite metamorphism of the gabbros and dykes they show similarities to the average N-MORB of Sun and McDonough (1989), as manifested by flat to slightly depleted LREE patterns on N-MORB-normalised REE plots and multi-element plots (Figure 8) [e.g. $(La/Sm)_{N\text{-}MORB} \approx 1$, $(La/Nb)_{N\text{-}MORB} \approx 1$]. This is in marked contrast with arc-related lithologies, which have characteristic negative Nb, Ta, and Ti anomalies and enriched LREE (Perfit *et al.* 1980; Pearce 1982). The positive Eu anomalies in all but one of the gabbros are consistent with plagioclase accumulation. A similar phenomenon is observed in the dykes. One gabbro has elevated abundances of incompatible elements with negative Eu and Ti anomalies consistent with being formed by late stage more-evolved melts that have lost plagioclase and magnetite. The variable enrichments in Rb, Ba and Sr displayed by the gabbros and dykes are probably due to alteration/metamorphism, although at least part of the positive Sr and Ba spikes may reflect plagioclase accumulation. The majority of gabbros and dykes display a distinctive negative Zr and Hf anomaly. This phenomenon appears to correlate well with modal plagioclase. The greater the plagioclase content (i.e. the more positive the Eu anomaly), the stronger the negative Zr–Hf anomalies. It is observed in Figure 8 that as the Eu spike flattens out the Zr–Hf trough also disappears, but when a negative Eu anomaly is observed a corresponding Zr and/or Hf spike is present. This negative correlation is demonstrated in Figure 9 where $Hf^* [Hf/(Sm + Gd)/2]_{N\text{-}MORB}$ is plotted against $Eu^* [Eu/(Sm + Gd)/2]_{N\text{-}MORB}$. This correlation may be explained using mineral/melt partition coefficients (K_D). The K_D values for Zr and Hf between plagioclase and basaltic melts are 0.048 and 0.051, respectively (Rollinson 1993). These elements are therefore highly incompatible in the mineral and are thus preferentially retained in the melt. The K_D

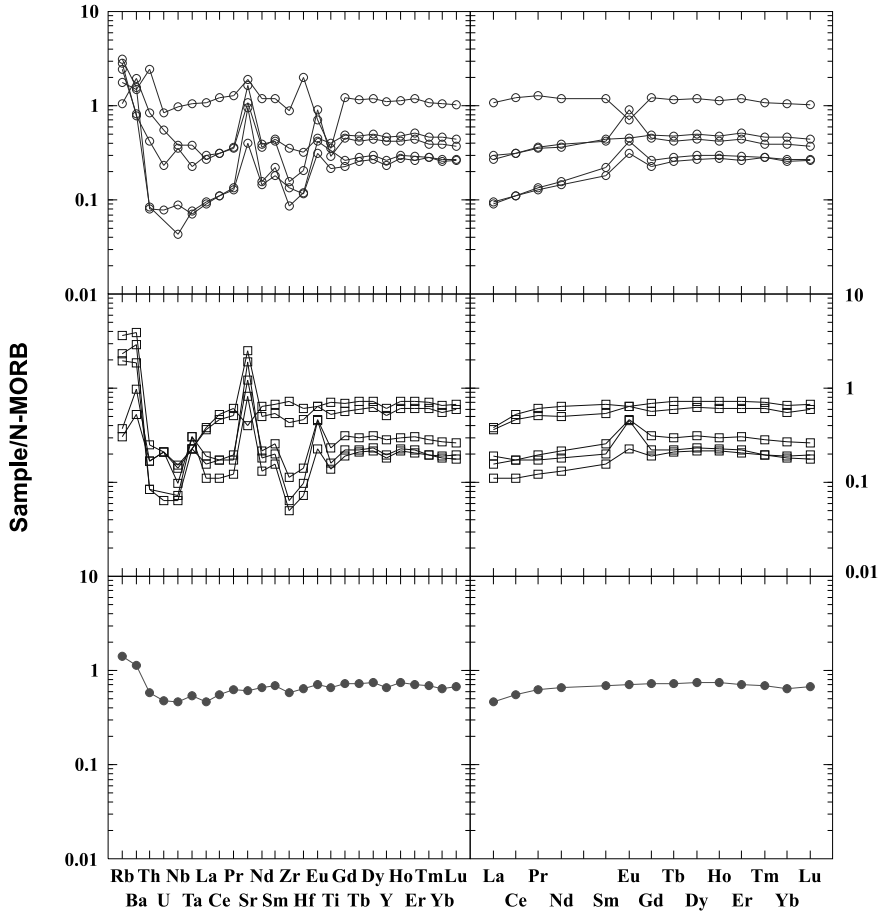

Figure 8 N-MORB-normalised incompatible multi-element (left) and rare-earth element (right) diagrams of the mafic rocks. Note the close similarities between the average N-MORB (Sun & McDonough 1989) (i.e. a uniform straight line running across the diagram at an elemental concentration level of 1 (not shown)) and the Marlborough basalt. ○, gabbro; □, dolerite; ●, basalt.

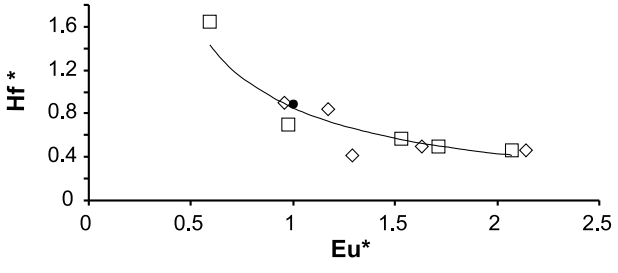

Figure 9 Hf* $[Hf/(Sm + Gd)/2]_{N\text{-}MORB}$ *vs* Eu* $[Eu/(Sm + Gd)/2]_{N\text{-}MORB}$ for rocks of basaltic magmatism. A good correlation is observed between positive Eu anomalies (i.e. Eu* > 1) and negative Hf anomalies (i.e. Hf* < 1) and vice versa. This corresponds with modal plagioclase cumulation and fractionation, respectively (see text for details). □, gabbro; ◇, dolerite; ●, basalt.

values for Sm and Gd are greater at 0.067 and 0.063, respectively, thus they are not as incompatible in plagioclase as Zr and Hf. Therefore, in the plagioclase-rich cumulates, Zr and Hf are more depleted, producing the observed negative anomalies with respect to Sm and Gd.

Basaltic enclaves in the gabbro are interpreted to be trapped liquid of primitive composition. One such analysed enclave has $Mg/(Mg + Fe^{2+}) = 0.71$ and a moderate TiO_2 content (0.82%). The CIPW normative mineralogy of this liquid indicates an olivine tholeiite. The enclave is characterised by high concentrations of compatible elements such as Co (43 ppm), Cr (326 ppm), V (197 ppm) and Sc (33 ppm), which together with a high Mg#, suggest a composition of quite primitive melt. Trace-element abundances (Figure 8) are typical of N-MORB derived by a moderate extent (10–20%) of melting from an incompatible depleted lherzolite source (Niu 1997; Niu & Batiza 1997) [Nb/Ta = 15.4, Nb/U = 49.7, Ce/Pb = 25.3, Th/Yb = 0.04, $(La/Sm)_{N\text{-}MORB} = 0.67$, $(La/Nb)_{N\text{-}MORB} = 1.0$]. The elevated abundances of mobile Rb and Ba could be due to alteration.

Sm–Nd GEOCHRONOLOGY

Analytical techniques

Sm–Nd isotope analysis was conducted in the ultra-clean radiogenic isotope laboratory at the University of Queensland. Samples (~100–300 mg) were first treated for several hours with 24 N HF and 7 N HNO_3 in open Teflon capsules to dissolve the major silicates. A mixed ^{149}Sm–^{150}Nd spike was added to a second HF and HNO_3 batch and samples were placed into steel-jacketed Teflon bombs at ~180°C. After 2 days complete dissolution was achieved. REE were separated using preconditioned cation-exchange columns with 2.5 N HCl and 6 N HCl as eluants. Separation of Nd and Sm from the rest of the REE was performed on a hydrogen di-ethylhexylphosphate (HDEHP) medium. Nd and Sm isotopes were measured on a Fisons VG Micromass 54-30 Sector multicollector mass spectrometer operating in

static mode. Measured $^{143}Nd/^{144}Nd$ ratios were normalised to $^{146}Nd/^{144}Nd = 0.7219$ to correct for mass fractionation. Repeat measurements of Ames® Nd metal standard ($n = 18$) over the time period of the study yielded $^{143}Nd/^{144}Nd = 0.511976 \pm 20$ (2σ). The Nd data were normalised to the mean of $^{143}Nd/^{144}Nd = 0.511971 \pm 9$ (2σ) previously obtained from Ames® Nd metal by dynamic analysis. Repeated isotope dilution analyses of BCR-1 using our ^{149}Sm–^{150}Nd-enriched spike gave mean Nd and Sm concentrations of 28.63 ± 9 and 6.54 ± 3 μg g^{-1}, respectively, and isotopic ratios of $^{147}Sm/^{144}Nd = 0.1382 \pm 3$ and $^{143}Nd/^{144}Nd = 0.512647 \pm 9$. Regression of Nd isotopic data followed the method of York (1969) and errors on isochron age and Nd isotopic ratio were calculated following the procedure of Fletcher and Rosman (1982). All errors in age and isotopic data quoted in this study are 2σ values. The initial epsilon neodymium [$\epsilon_{Nd}(t)$] parameter was calculated from the isochron intercept with reference to CHUR values of $^{147}Sm/^{144}Nd = 0.1967$ and $^{143}Nd/^{144}Nd = 0.512638$.

RESULTS

Five cogenetic whole-rock mafic samples of the ophiolite were analysed for Sm–Nd isotopes (Table 3). These samples include one basalt, two dolerites and two gabbros chosen to represent the crustal section of the ophiolite. All samples contain lower greenschist facies assemblages partially overprinting primary clinopyroxene and plagioclase. They have smooth (excluding Eu) N-MORB-like REE patterns indicating primary abundances. The data (Figure 10) define a well-constrained (MSWD = 0.21) isochron on $^{143}Nd/^{144}Nd$–$^{147}Sm/^{144}Nd$ space that yields a crystallisation age of 562 ± 22 Ma. The initial ratio obtained from this fit is $^{143}Nd/^{144}Nd_i = 0.512369 \pm 7$ corresponding to $\epsilon_{Nd}(t) = +8.9 \pm 0.15$, which is very similar to the estimated Nd isotopic value of the upper mantle at 562 Ma [$\epsilon_{Nd}^{(562\ Ma)} = +8.7$] using the Sm–Nd terrestrial evolutionary model of Nägler and Kramers (1998). Thus, the very depleted Nd-isotope signature further argues that the Marlborough ophiolite originated from a depleted MORB mantle source, as demonstrated by the mineralogical and trace-element data presented above.

DISCUSSION

The *ca* 560 Ma crystallisation age indicates that rocks of the Marlborough ophiolite are some of the oldest rocks so far identified throughout the New England Fold Belt. Mineralogical, geochemical and isotopic data all argue persuasively that the Marlborough ophiolite was formed at a sea-floor spreading centre. This is in contrast to other occurrences of ophiolitic rocks found throughout the New England Fold Belt (Aitchison *et al.* 1994) whose origin is interpreted to be associated with an arc environment (Aitchison *et al.* 1992; Aitchison & Ireland 1995; Yang & Seccombe 1997).

Geochemically, it can be very difficult to distinguish between rocks that were formed at an ocean ridge and those that were formed in a marginal basin (Saunders *et al.* 1980). This is particularly true for crustal rocks of the Marlborough ophiolite as there is actually only one analysis interpreted to represent primitive liquid composition.

Table 3 Sm–Nd isotopic results for whole rocks.

	Rock type	Sm (ppm)	Nd (ppm)	$^{147}Sm/^{144}Nd$	$^{143}Nd/^{144}Nd$	$\epsilon_{Nd}(0)$	$\epsilon_{Nd}(562)$	ϵ_{Nd}(isochron)
Marlborough Ophiolite								
MB3	Dolerite	0.65	1.61	0.2532	0.513299	+12.89	+8.85	
MB8	Basalt	1.78	4.52	0.2275	0.513204	+11.04	+8.84	
MB9	Gabbro	3.27	9.22	0.2146	0.513161	+10.20	+8.93	$+8.89 \pm 0.15$
MB114	Gabbro	0.53	1.12	0.2864	0.513424	+15.33	+8.90	
MB116a	Dolerite	2.54	6.71	0.2288	0.513210	+11.16	+8.86	

Errors used in isochron calculation are true analytical errors, including sources of such errors as instrumental reproducibility. These are 0.0016% on $^{143}Nd/^{144}Nd$ ratios and 0.5% on $^{147}Sm/^{144}Nd$ ratios.

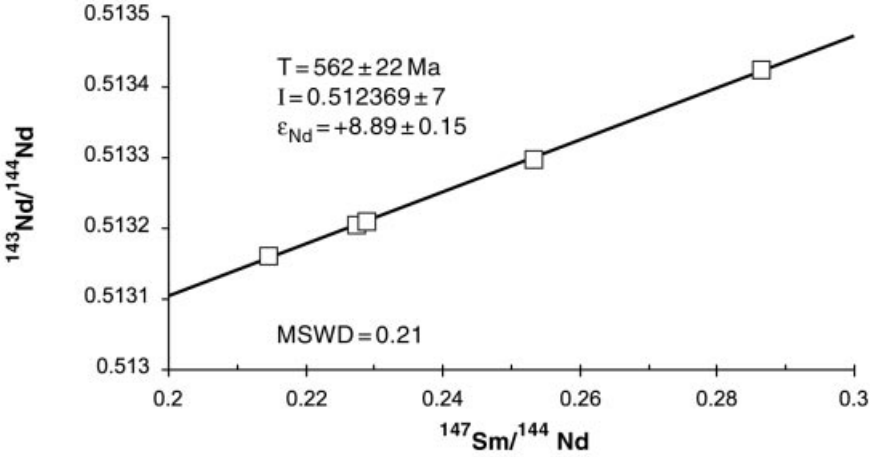

Figure 10 Sm–Nd isochron diagram constructed for mafic rocks of the Marlborough ophiolite. T, age of isochron; I, initial $^{143}Nd/^{144}Nd$; ϵ_{Nd}, initial epsilon Nd value. All reported errors are at 2σ. Note that the symbol size used is larger than the error bars for each sample.

This basalt is, however, more depleted than the average N-MORB (as are the dolerites and gabbros) with no substantial evidence for 'input' from slab-derived subduction fluids rich in LILE, as may be expected in backarc environments where source heterogeneity is probable from subducted components associated with the arc (Saunders *et al.* 1980; Saunders & Tarney 1984). Positive Rb and Ba anomalies in the basalt of the Marlborough ophiolite are probably due to metamorphism/alteration as they do not represent a systematic increase in LILE (e.g. no apparent increase in Sr concentration). Nor are there any corresponding negative HFSE anomalies as would be expected in rocks from a subduction-dominated environment. The consistency of the depleted MORB-like signatures in the Marlborough mafic rocks is further supported by Nd isotopes typical of depleted mantle values at the time of formation. A further geochemical argument for formation at an ocean ridge comes from the mantle section itself, which retains relict igneous minerals with compositions similar to those from abyssal peridotites. Thus, the consistency of depleted MORB-like rocks and the absence of transitional, enriched or arc-related lavas of a similar age suggests that the ophiolite was once part of a Late Neoproterozoic ocean basin, perhaps extensive, which must have existed to the east of the Tasman Line. This suggests that the New England Fold Belt may have developed on oceanic crust and accreted during progressive cratonisation of the east Australian margin.

The next oldest rocks dated from the New England Fold Belt are from ophiolitic rocks along the Peel Fault System and are *ca* 530 Ma (Aitchison *et al.* 1992) and interpreted to have formed in a backarc basin (Yang & Seccombe 1997). This places constraints on the development of eastern Australia and may suggest an oceanward 'outstepping' of the subduction zone that was initiated at *ca* 580 Ma due to the subduction of oceanic lithosphere beneath the cratonic margin of Australia (Fergusson *et al.* 1998). In this scenario, the oceanic Marlborough ophiolite may have been isolated on the overriding plate and later passively accreted to the continent. Such an oceanward migration of the arc is envisaged to have occurred at *ca* 540 Ma as recorded by deformation and metamorphism in the Anakie Inlier (Fergusson *et al.* 1998). Deformational structures from this event show mylonitic features and widespread stretching lineations that indicate tectonic transport to the east-northeast (Withnall *et al.* 1996; Fergusson *et al.* 1998).

ACKNOWLEDGEMENTS

MCB and TAH carried out field mapping and sampling in 1995–1997 as part of two complementary PhD projects. The study project of MCB was funded by an ARC grant to YN and RJH. MCB and TAH would like to thank Queensland Metal Corporation, in particular Darcy Milburn, for assistance and support in the field. MCB would also like to extend his appreciation to Frank Audsley and Sharyn Price for helping with major element analysis and to Ron Rasch for his training, persistence and tireless help on the electron microprobe. Marcel Regelous, Immo Wendt and Ken Collerson are acknowledged for their assistance in Thermal Ionisation Mass Spectrometry. Balz Kamber is thanked for his comments on an early draft of the manuscript. Constructive formal reviews by Cecil Murray and Peter Cawood were very helpful and led to improved versions of earlier manuscripts.

REFERENCES

Aitchison J. C., Blake Jr. M. C., Flood P. G. & Jayko A. S. 1994. Palaeozoic ophiolitic assemblages within the southern New England Orogen of eastern Australia: implications for growth of the Gondwana margin. *Tectonics* **13**, 1135–1149.

Aitchison J. C. & Ireland T. R. 1995. Age profile of ophiolitic rocks across the Late Palaeozoic New England Orogen, New South Wales: implications for tectonic models. *Australian Journal of Earth Sciences* **42**, 11–23.

Aitchison J. C., Ireland T. R., Blake Jr. M. C. & Flood P. G. 1992. 530 Ma zircon age for ophiolite from the New England Orogen: oldest rocks known from eastern Australia. *Geology* **20**, 125–128.

Allen C. M., Williams I. S., Stephens C. J. & Fielding C. R. 1998. Granite genesis and basin formation in an extensional setting: the magmatic history of the northernmost New England Orogen. *Australian Journal of Earth Sciences* **45**, 875–888.

Bodinier J. L. 1990. Mechanisms of mantle metasomatism: geochemical evidence from the Lherz orogenic peridotite. *Journal of Petrology* **31**, 597–628.

Bruce M. C. & Niu Y. 2000. Evidence for Palaeozoic magmatism recorded in the Late Neoproterozoic Marlborough ophiolite, New England Fold Belt, central Queensland. *Australian Journal of Earth Sciences* **47**, 1065–1076.

Campbell I. H., Lesher C. M., Coad P., Franklin J. M., Gorton M. P. & Thurston P. C. 1984. Rare earth element mobility in alteration pipes below massive sulfide deposits. *Chemical Geology* **45**, 181–202.

Cann J. R. 1969. Spilites from the Carlsberg Ridge, Indian Ocean. *Journal of Petrology* **10**, 1–19.

Cawood P. A. & Leitch E. C. 1985. Accretion and dispersal tectonics of the southern New England Fold Belt, eastern Australia. *In:* Howell D. G. ed. *Tectonostratigraphic Terranes of the Circum-Pacific Region,* Vol. 1. pp. 481–492. Circum-Pacific Council for Energy and Mineral Resources, Earth Science Series, Houston.

Day R. W., Murray C. G. & Whitaker W. G. 1978. The eastern part of the Tasman Orogenic Zone. *Tectonophysics* **48**, 327–364.

Denton M. G. 1994. The metamorphic petrology and geochemistry of the Princhester area, Marlborough, central-eastern Queensland. BSc (Hons) thesis, University of Queensland, Brisbane (unpubl.).

Dick H. J. B. & Bullen T. 1984. Chromium spinel as a petrogenetic indicator in abyssal and alpine-type peridotites and spatially associated lavas. *Contributions to Mineralogy and Petrology* **86**, 54–76.

Fergusson C. L., Green T. J., Fanning M. C., Carr P. F., Withnall I. W. & Crouch S. B. S. 1998. Neoproterozoic age for deformation and metamorphism in the Anakie Inlier, central Queensland: implications for opening of the Pacific Ocean and timing of the Delamarian-Ross Orogeny. *Geological Society of Australia Abstracts* **49**, 141.

Fletcher I. R. & Rosman K. J. R. 1982. Precise determination of initial ϵ_{Nd} from Sm–Nd isochron data. *Geochimica et Cosmochimica Acta* **46**, 1983–1987.

Frey F. A. 1984. Rare earth element abundances in upper mantle rocks. *In:* Henderson P. ed. *Rare Earth Element Geochemistry*, pp 153–203. Developments in Geochemistry **2**. Elsevier, Amsterdam.

Gomez Cebria S. M. 1990. A program for pyroxene classification and calculation of end-members. *American Mineralogist* **75**, 1426–1427.

Gruau G., Bernard-Griffiths J. & Lécuyer C. 1998. The origin of U-shaped rare earth patterns in ophiolite peridotites: assessing the role of secondary alteration and melt/rock reaction. *Geochimica et Cosmochimica Acta* **62**, 3545–3560.

Haskin L., Frey F. A., Schmitt R. A. & Smith R. H. 1966. Meteoric, solar and terrestrial rare-earth distributions. *Physics and Chemistry of the Earth* **7**, 169–321.

Hébert R., Serri G. & Hékinian R. 1989. Mineral chemistry of ultramafic tectonites and ultramafic to gabbroic cumulates from the major oceanic basins and northern Apennine ophiolites (Italy)—a comparison. *Chemical Geology* **77**, 183–207.

HOLCOMBE R. J., STEPHENS C. J., FIELDING C. R. *ET AL.* 1997a. Tectonic evolution of the northern New England Fold Belt: Carboniferous to Early Permian transition from active accretion to extension. *In:* Ashley P. M. & Flood P. G. eds. *Tectonics and Metallogenesis of the New England Orogen*, pp. 66–79. Geological Society of Australia Special Publication **19**.

HOLCOMBE R. J., STEPHENS C. J., FIELDING C. R. *ET AL.* 1997b. Tectonic evolution of the northern New England Fold Belt: the Permian-Triassic Hunter-Bowen event. *In:* Ashley P. M. & Flood P. G. eds. *Tectonics and Metallogenesis of the New England Orogen*, pp. 52–65. Geological Society of Australia Special Publication **19**.

HUMPHRIS S. E. 1984. The mobility of the rare earth elements in the crust. *In:* Henderson P. ed. *Rare Earth Element Geochemistry*, pp. 317–342. Elsevier, New York.

ISHIWATARI A. 1985. Igneous petrogenesis of the Yakuno Ophiolite (Japan) in the context of the diversity of ophiolites. *Contributions to Mineralogy and Petrology* **89**, 155–167.

JAGOUTZ E., PALME H., BADDENHAUSEN H. *ET AL.* 1979. The abundances of major, minor and trace elements in the earth's mantle as derived from primitive ultramafic nodules. *Proceedings of the Lunar and Planetary Science Conference* **10**, 2031–2050.

KORSCH R. J., JOHNSTONE D. W. & WAKE-DYSTER K. D. 1997. Crustal architecture of the New England Orogen based on deep seismic reflection profiling. *In:* Ashley P. M. & Flood P. G. eds. *Tectonics and Metallogenesis of the New England Orogen*, pp. 29–51. Geological Society of Australia Special Publication **19**.

KWIECIEN W. 1990. *Silicate Rock Analysis by AAS*. School of Geology, Queensland University of Technology, Brisbane.

LEITCH E. C. 1974. The geological development of the southern part of the New England Fold Belt. *Journal of the Geological Society of Australia* **21**, 133–156.

LEITCH E. C. 1975. Plate tectonic interpretation of the Palaeozoic history of the New England Fold Belt. *Geological Society of America Bulletin* **86**, 141–144.

LESHER C. M., GIBSON H. L. & CAMPBELL I. H. 1986. Composition–volume changes during hydrothermal alteration of andesite at Buttercup Hill, Noranda district, Quebec. *Geochimica et Cosmochimica Acta* **50**, 2693–2705.

MURRAY C. G. 1969. The petrology of the ultramafic rocks of the Rockhampton district, Queensland. *Geological Survey of Queensland* **343**, 1–13.

MURRAY C. G. 1974. Alpine-type ultramafics in the northern part of the Tasman Geosyncline—possible remnants of Palaeozoic ocean floor. *In*: Denmead A. K., Tweedale G. W. & Wilson A. F. eds. *The Tasman Geosyncline—a Symposium*, pp. 161–181. Geological Society of Australia, Queensland Division, Brisbane.

NÄGLER T. F. & KRAMERS J. D. 1998. Nd isotopic evolution of the upper mantle during the Precambrian: models, data and the uncertainty of both. *Precambrian Research* **91**, 233–252.

NIU Y. 1997. Mantle melting and melt extraction processes beneath ocean ridges: evidence from abyssal peridotites. *Journal of Petrology* **38**, 1047–1074.

NIU Y. & BATIZA R. 1997. Trace element evidence from seamounts for recycled oceanic crust in the Eastern Pacific mantle. *Earth and Planetary Science Letters* **148**, 471–483.

NIU Y. & HÉKINIAN R. 1997. Basaltic liquids and harzburgitic residues in the Garrett Transform: a case study at fast-spreading ridges. *Earth and Planetary Science Letters* **146**, 243–258.

NIU Y., LANGMUIR C. H. & KINZLER R. J. 1997. The origin of abyssal peridotites: a new perspective. *Earth and Planetary Science Letters* **152**, 251–265.

NIU Y. & LESHER C. M. 1991. Hydrothermal alteration of mafic metavolcanic rocks and genesis of Fe–Zn–Cu sulfide deposits, Stone Hill district, Alabama. *Economic Geology* **86**, 983–1001.

NORRISH K. & CHAPPELL B. W. 1977. X-ray fluorescence spectrometry. *In:* Zussman J. ed. *Physical Methods in Determinative Mineralogy*, pp 201–272. Academic Press, London.

O'HANLEY D. S. 1995. *Serpentinites: Recorders of Tectonic and Petrological History*. Oxford Monographs on Geology and Geophysics **32**. Oxford University Press, New York.

PEARCE J. A. 1976. Statistical analysis of major element patterns in basalts. *Journal of Petrology* **17**, 15–43. John Wiley and Sons, London.

PEARCE J. A. 1982. Trace element characteristics of lavas from destructive plate boundaries. *In:* Thorpe R. S. ed. *Andesites: Orogenic Andesites and Related Rocks*, pp. 525–548.

PERFIT M. R., GUST D. A., BENCE A. E., ARCULUS R. J. & TAYLOR S. R. 1980. Chemical characteristics of island arc basalts: implications of mantle sources. *In:* Le Maitre R. W. & Cundari A. eds. *Chemical Characterisation of Tectonic Provinces*, pp. 227–256. *Chemical Geology* **30**.

ROLLINSON H. R. 1993. *Using Geochemical Data: Evaluation, Presentation, Interpretation*. Longman Scientific and Technical, New York.

SAUNDERS A. D. & TARNEY J. 1984. Geochemical characteristics and tectonic significance of back-arc basins. *In:* Kokelaar B. P. & Howells M. F. eds. *Marginal Basin Geology: Volcanic and Associated Sedimentary and Tectonic Processes in Modern and Ancient Marginal Basins*, pp. 59–76. Geological Society of London Publication **16**.

SAUNDERS A. D., TARNEY J., MARSH N. G. & WOOD D. A. 1980. Ophiolites as ocean crust or marginal basin crust; a geochemical approach. *In:* Panayiotou A. ed. *Proceedings of the International Ophiolite Symposium, Cyprus 1979*, pp. 193–204. Geological Survey Department, Cyprus.

SNOW J. E. & DICK H. J. B. 1995. Pervasive magnesium loss by marine weathering of peridotite. *Geochimica et Cosmochimica Acta* **59**, 4219–4235.

SUN S-S. & MCDONOUGH W. F. 1989. Chemical and isotopic systematics of oceanic basalts: implications for mantle composition and processes. *In:* Saunders A. D. & Norry M. J. eds. *Magmatism in Ocean Basins*, pp. 313–345. Geological Society of London Special Publication **42**.

THAYER T. P. 1967. Chemical and structural relations of ultramafic and feldspathic rocks in alpine intrusive complexes. *In:* Wyllie P. J. ed. *Ultramafic and Related Rocks*, pp 222-239. John Wiley and Sons, New York.

WICKS F. J. & O'HANLEY D. S. 1988. Serpentine minerals: structure and petrology. *In:* Bailey S. W. ed. *Hydrous phyllosilicates*, pp. 91–168. Reviews in Mineralogy **19**.

WITHNALL I. W., GOLDING S. D., REES I. D. & DOBOS S. K. 1996. K–Ar dating of the Anakie Metamorphic Group: evidence for an extension of the Delamarian Orogeny into central Queensland. *Australian Journal of Earth Sciences* **43**, 567–572.

YANG K. & SECCOMBE P. K. 1997. Geochemistry of the mafic and ultramafic complexes of the northern Great Serpentinite Belt, New South Wales: implications for first-stage melting. *In:* Ashley P. M. & Flood P. G. eds. *Tectonics and Metallogenesis of the New England Orogen*, pp 197–211. Geological Society of Australia Special Publication **19**.

YORK D. 1969. Least squares fitting of a straight line with correlated errors. *Earth and Planetary Science Letters* **5**, 320–324.

Received 1 November 1999; accepted 19 July 2000

APPENDIX 1: SAMPLE LOCATIONS

Sample	AMG coordinates	Sample	AMG coordinates
MB3	199083E; 7466100N	MB94	802850E; 7461492N
MB8	200525E; 7463560N	MB100	202017E; 7461432N
MB9	200525E; 7463560N	MB108	804165E; 7460352N
MB18	797456E; 7458616N	MB114	198697E; 7466460N
MB21	797509E; 7458463N	MB116a	198108E; 7466817N
MB88	803027E; 7461488N		

Marlborough (8852) and Princhester (8952) 1:100 000 sheets.